

Targeting mechanoresponsive proteins in pancreatic cancer: 4-hydroxyacetophenone blocks dissemination and invasion by activating MYH14

Alexandra Surcel, Eric S. Schiffhauer, Dustin G. Thomas, Qingfeng Zhu, Kathleen T. DiNapoli, Maik Herbig, Oliver Otto, Hoku West-Foyle, Angela Jacobi, Martin Kräter, Katarzyna Plak, Jochen Guck, Elizabeth M. Jaffee, Pablo A. Iglesias, Robert A. Anders, Douglas N. Robinson

Supplemental Materials

Supplemental materials include following:

Supplemental Materials and Methods

Table S1. NMII Concentration (n), nM

Fig. S1. Model systems to human pancreatic cancer.

Fig. S2. Scoring analysis and differential expression patterns of mechanoresponsive and non-mechanoresponsive paralogs in patient-derived IHC data.

Fig. S3: Measurement of endogenous expression of nonmuscle myosin II paralogs and the effect of knockdown, overexpression, and 4-HAP treatment on the expression of mechanobiome proteins.

Fig. S4. Pancreatic cancer cell lines are mechanically distinct from each other.

Fig. S5: Method for quantifying actin structures at the cellular cortex.

Fig. S6: 4-HAP decreases actin retrograde flow.

Fig. S7: 4-HAP treated livers show reduced surface tumor coverage.

Movie S1. Retrograde flow of an untreated AsPC-1 Sir-Act-stained cell.

Movie S2. Retrograde flow of a 4-HAP-treated AsPC-1 Sir-Act-stained cell.

Supplemental Materials and Methods

Construct Assembly

Myosin IIC_{pep}

Using pBiEx1-mCh-IIC tail fragment construct as template, a ~100 bp PCR product for the myosin IIC_{pep} was generated using the following primers:

Forward primer: 5' – AAAAAAGTCGACAGGAACCGGCTTCGACGC – 3'

Reverse primer: 5' – TTTTATAGCGGCCGCTCATAGTCGAAGACCTG – 3'

The product was inserted into the expression construct pEGFP-N3 (Addgene), replacing the GFP, and then sequenced to verify. Then, the plasmid was transfected into cells using FuGene HD transfection reagent (Promega, Madison, WI) using 1 µg of DNA for each plasmid and imaged 36 hrs post-transfection.

Immunohistochemistry of patient-derived samples

Antibodies and reagents

Antibodies used include: myosin IIA Poly19098 (BioLegend, 909801), myosin IIB CMII 23 from the Developmental Studies Hybridoma Bank (mouse; deposited by G. Conrad and A. Conrad, Kansas State University, Manhattan, KS) used for quantitative western blots, myosin IIB (D8H8) XP (Cell Signaling Technology, #8824) used for immunohistochemistry staining of human samples, myosin IIC (D4A7) (Cell Signaling Technology, #8189), α-actinin 1 (OTI7A4) (OriGene, TA500072), α-actinin 4 (G-4) (Santa Cruz Biotechnology, sc-390205), filamin A (Cell Signaling Technology, #4762), filamin B [N1] (GeneTex, GTX101206), and β-actin (8H10D10) (Cell Signaling Technology, #3700).

Immunohistochemistry staining

Immunohistochemistry was performed as previously described (1). In short, warmed slides were deparaffinized in sequential xylene washes, followed by 100%, 95%, and 70% ethanol washes. Slides were incubated in 0.3% H₂O₂ in MeOH for 20 min, then washed twice in water. Slides are steamed in citrate buffer (pH 6.0) for 35 min. Cooled slides were washed twice in water and three times in TBST (50 mM Tris-Cl, pH 7.5; 150 mM NaCl; 0.1% Tween-20). Slides were edge

dried with a Kimwipe and Serum Free Protein Block Dako X0909 (Agilent, Santa Clara, CA) was applied for 10 min. Dried slides were incubated with primary antibody for 1 hr at 22°C, washed in TBST three times, air-dried, and incubated in secondary antibody (Dako), K400111-2, EnVision+, HRP. Mouse or K401111 -2, En Vision+ HRP. Rabbit 1100 tests (Dako) for 20 min at 22°C. Slides were washed three times in TBST, followed by incubation for 2-3 min in DAB+. Stained slides were washed with water, incubated for 15 sec in hematoxylin (Sigma), and washed first with water, then ethanol, and water again, incubated in acid alcohol, with a final water rinse. Slides are incubated in bluing water, washed, and dehydrated in 70% ethanol for 2 min, 100% ethanol for 2 min, and xylenes for 1 min.

Scoring and imaging

Slides were scanned using the Hamamatsu Digital Scanner and white balanced in Adobe Photoshop (Adobe Systems, Inc). Samples were scored based on both intensity of staining and surface area of duct covered by staining. Each slide was visualized in its entirety to determine uniformity of staining. Five cancerous ducts and five normal ducts (when present) were selected at random. Ducts with no staining were given a 0/0, ducts with intense staining on over 50% of the ductal surface were given a 2/2, with intermediate staining lying between these two endpoints. Ducts with intense staining on less than 50% of their area were scored as 2/1, ducts with moderate staining on over 50% of their ductal surface were scored as 1/2, and those with moderate staining on less than 50% of their ductal surface were scored as 1/1. To quantify the distribution of staining across all patient samples (**Fig. 2B**), individual duct scores were reassigned as follows: 0/0 as a 1, 1/1 as a 2, 1/2 as a 3, 2/1 as a 4, and 2/2 as a 5 (**Fig. S2A**). Slides were imaged on NDP.View2 NanoZoomer Digital Pathology (NDP.View2, Hamamatsu Photonics, Japan).

Quantification of cellular myosin II paralog concentrations by western analysis

Myosin II tail fragment protein purification

Bacterial expression plasmids coding for an N-terminal 6xHis tag, fused to the mCherry fluorophore, fused to the assembly domains of human myosin-IIA (residues 1722-1960), human myosin-II B (residues 1729-1976), and mouse myosin-II C (residues 1782-2033) were generated in pBiEx1 using standard cloning techniques. Proteins were expressed in BL-21 Star™ (DE3)

(Invitrogen) *E. coli* in LB shaking culture overnight at room temperature. Bacteria were harvested by centrifugation and lysed by lysozyme treatment followed by sonication, and the lysate was clarified by centrifugation. Polyethyleneimine (PEI) was added to a final concentration of 0.1% to precipitate nucleic acids, which were then removed by centrifugation. The myosin-II constructs were precipitated by adding ammonium sulfate to 50% saturation and centrifuging. The pellet was resuspended in column running buffer, dialyzed against the same for a minimum of 4 hrs, clarified by centrifugation and filtration, and run on a Ni-NTA metal affinity column, followed by a sizing column. The constructs were then concentrated and further purified by dialyzing against assembly buffer (10 mM HEPES, pH 7.1, 50 mM NaCl) until precipitate formed, followed by centrifugation and resuspension of the pellet in storage buffer (10 mM HEPES, pH 7.1, 500 mM NaCl). Protein purity was verified by SDS-PAGE followed by Coomassie Blue staining, and concentration was quantified by UV absorbance using the calculated extinction coefficient for each protein's amino acid sequence.

Quantitative western analysis

Cells were trypsinized and counted, then centrifuged into pellets containing 5×10^5 cells each. These pellets were washed in 1xPBS and recentrifuged, then lysed in 75 μ L RIPA lysis buffer plus 15 μ L 6xSDS sample buffer. Due to cell volume and residual PBS, the total lysate volume reached 100 μ L. 10 μ L of lysate was added to each well of a 7% SDS-PAGE gel, or the equivalent of 5×10^4 cells/well. In addition, each well was spiked with a known quantity of purified myosin II tail fragment, containing the epitope region for the antibodies used, with sequential 2-fold dilutions. A 7% gel was used because it allowed for optimal transfer of both the large molecular weight endogenous myosin II and the smaller molecular weight purified tail fragment out of the gel. Transfer was most effective at a constant 45V for 16 hrs, using PVDF membranes to prevent smaller protein pass-through and verifying complete transfer of larger proteins by performing a Coomassie stain to verify that no protein was left in the gel following transfer. The average volume of an individual cell for each cell type was determined from the micropipette aspiration images, where cell radius is measured, and assuming the cell shape to be a sphere prior to aspiration. For each experiment, a standard curve was created from the spiked tail fragment to determine the total number of moles of endogenous myosin II in each lane. The number of cells per lane multiplied by the average volume of a single cell gave the total cell

volume per lane, and concentration was determined as a ratio of these two values. Antibodies used were the same as those for immunohistochemistry (described above).

Quantification of myosin IIC isoforms via cQPCR

RNA was isolated from each cell line at passage number 3 using TRIzol reagent and protocol (Invitrogen). qTPCR was performed as previously described for myosin IIC isoforms (2), using Sybr green master mix for real time PCR (Applied Biosystems, Grand Island, NY). Each sample was measured in triplicate. Counts were normalized relative to GAPDH counts for each cell line. Primers for GAPDH used as a positive control were:

Forward: CATCAATGGAAATCCCATCA

Reverse: GACTCCACGACGTACTCAGC

Mammalian cell sedimentation protocol

Panc10.05 cells were trypsinized and washed in 1ml of PBS. The pellet was resuspended in 100 μ L of lysis buffer (50 mM 1,4-piperazine diethane sulfonic acid (pH 6.8), 46 mM NaCl, 2.5 mM EGTA, 1 mM MgCl₂, 1 mM ATP, 0.5% Triton X100, and protease inhibitor mixture (PMSF, N-a-tosyl-L-lysine chloromethyl ketone hydrochloride, aprotinin)). Samples were vortexed briefly and incubated on ice for 10 min, followed by centrifugation at 15,000 \times g for 5 min at 4 °C. The pellet was resuspended in 100 μ L of lysis buffer and both the pellet and supernatant fractions were passed through a qIA shredder column (QIAGEN), then heated with 2X sample buffer to 95 °C for 3 min with RNaseA. Samples were loaded on a 15% SDS/polyacrylamide gel. Western blot analyses of myosin IIC were performed.

Micropipette aspiration assay for mechanoreponse and mechanics measurements and real-time deformability cytometry measurements

The instrumental and experimental setups have been described previously (3,4). MPA assays and RT-DC measurements were all carried out in growth media for cortical tension measurements or Leibovitz L-15 media (Gibco) when fluorescence was quantified.

Measurements of mechanosensory accumulation of proteins

A pressure difference was generated by adjusting the height of a motor-driven water manometer. Mammalian cells expressing desired fluorescent proteins were loaded into the observation chamber, which was filled with Leibovitz L-15 Medium without phenol red (Gibco). Cells were deformed using a pressure of $0.3 \text{ nN}/\mu\text{m}^2$ and recorded for 5 min. Pressures higher than this often led to blebbing or the separation of cell membrane from the cortex. All cells which demonstrated blebbing during recording were discarded. Images were collected with an Olympus IX81 microscope equipped with MetaMorph software and analyzed using ImageJ (National Institutes of Health). After background correction, the fluorescence intensity at the accumulation site inside the micropipette was normalized against the opposite cortex of the cell (I_p/I_o). The peak I_p/I_o value during the 5 min timecourse was then normalized to the I_p/I_o value at $t=0$ to adjust for initial variations in cortical fluorescence (Normalized I_p/I_o).

Cortical tension measurements

Pressure was applied to the cell cortex with a micropipette (6- to 8- μm radius; R_p) to the equilibrium pressure (ΔP), where the length of the cell inside the pipette (L_p) was equal to R_p . The effective cortical tension (T_{eff}) was calculated by applying the Young–Laplace equation: $\Delta P = 2T_{\text{eff}} (1/R_p - 1/R_c)$, where R_c is the radius of the cell and ΔP is the equilibrium pressure when $L_p = R_p$ (4). Images were collected with an Olympus IX81 microscope equipped with MetaMorph software and analyzed using ImageJ (rsb.info.nih.gov/ij).

Real-time deformability cytometry

Mechanical measurements of thousands of cells were obtained as previously described (3). Approximately 10^6 cells were trypsinized, spun, resuspended in media, and incubated at 37°C for 10 min prior to loading onto the AcCellerator (Zellmechanik Dresden), using a 30- μm channel. In this device, cells are run through a microfluidic chip with a constriction channel, where the deformation and cell size data was collected in real-time at three different flow-rates and analyzed using ShapeOut 0.8.7 (Zellmechanik Dresden; available at <https://github.com/zellmechanik-dresden/ShapeOut>). Differences in deformation were plotted as a probability distribution in R (r-project.org/), and the elastic modulus, based on the median

of the deformation and area populations, the channel width, viscosity, and flow rate was calculated (5).

Imaging and Image Analysis

Imaging was performed in culture media or Leibovitz L-15 media without phenol red (Gibco) and 10% FBS for mechanoresponse and lattice light sheet experiments. Confocal imaging was performed on a Zeiss AxioObserver LSM800 microscope with a 63X (1.4 N.A.) objective (Carl Zeiss). Epifluorescence imaging was performed with an Olympus IX81 microscope using a 40X (1.3 N.A.) objective and a 1.6X optovar (Olympus), as previously described. Image analysis was performed with ImageJ (rsb.info.nih.gov/ij). Datasets were independently analyzed by multiple investigators.

Single cell assays

2D random migration

AsPC-1 cells were plated at a sub-confluent concentration in a 24-well tissue culture plate (<5,000 cells) and incubated overnight in growth media (see above). Prior to imaging, cells media was changed to Leibovitz L-15 media without phenol red (Gibco) containing 10% FBS and 1% penicillin/streptomycin. Cells were imaged using Molecular Devices IXM High Content Imager 10X objective (NA) every 30 min for 24 hrs. Cell roundness, velocity and area were quantified using ImageJ.

Retrograde flow

AsPC-1 cells were grown on collagen I-coated (50 μ g/ml) 5-mm coverslips for 16 hrs and then treated with 100 nM SiR-Actin (Cytoskeleton, Inc) and 1 μ M Verapamil for 4 hrs in Leibovitz L-15 without phenol red media, with or without 4-HAP (500 nM). Coverslips were transferred to the imaging chamber of the Lattice Light-Sheet Microscope (LLSM) (Intelligent Imaging Innovations) containing fresh Leibovitz L-15 media without SiR-Actin and verapamil plus the corresponding 4-HAP concentration. Cells were imaged for 3-5 min at 2-3-sec intervals, 50-150 planes per 3D stack, with a Nikon CF175 Achromat 25X/1.1 water-dipping objective. Retrograde actin flow was measured using ImageJ (rsb.info.nih.gov/ij). Datasets were independently analyzed by multiple investigators.

Transwell assays

AsPC-1 cells were plated in 6.5-mm PET membrane transwell inserts with 8- μ m pores (Costar #3464) in a 24-well plate at a concentration of 5,000 cells per well. Cells were allowed to adhere overnight in AsPC-1 media. Cell media was then changed to serum-free RPMI 1640 to starve cells for 18 hrs. Following starvation, cells were stimulated by changing media in the top chamber to fresh serum-free RPMI 1640 \pm 500 nM 4-HAP and complete AsPC-1 media \pm 500 nM 4HAP. Cells were then incubated for 24 hrs at 37°C/5% CO₂ and then fixed in 4% paraformaldehyde, permeabilized in 0.1% Triton X-100 and stained with 1 μ g/ml DAPI. Prior to imaging, the top chamber was swabbed with a cotton-tip swab and washed to remove cells that did not translocate. A total of five random fields per transwell insert were imaged using a 10X objective (NA) and number of nuclei were averaged.

Tissue spheroid generation, staining, and quantification

Tissue spheroid generation

Tissue spheroids were grown by plating Panc10.05 cells on a drop of Matrigel (Becton-Dickinson) in an 8-well slide chamber (6,500 cells per well) and grown in RPMI 1640 media (2% serum, 2% matrigel, and 10 ng/ml EGF). Spheroids were grown for 14 days with regular media changes, then aspirated off the surface of the matrigel, washed with ice-cold PBS with mild centrifugation (4,000 RCF, 5 min). For all 2D spreading assays, spheroids were then plated on 50 μ g/ml collagen-coated 8-well coverslips (MatTek) and incubated for 48 hrs in complete PANC media with 500 nM 4-HAP or PBS control. For 3D invasion assays, spheroids were resuspended in a 1.5 mg/ml collagen solution (Life Technologies) and then plated in 8-well chambered coverslips. Spheroids were incubated in complete PANC media with 500 nM 4-HAP or PBS control for 48 hrs. All spheroid samples were fixed in 4% paraformaldehyde for 15 min at 25°C and permeabilized in 0.1% Triton X-100 for 15 min at 25°C. The actin cytoskeleton was visualized with rhodamine-phalloidin (5 μ M) for 30 min. Two-dimensional spreading was visualized with Olympus Spinning disk microscope (40X oil objective, 1.3NA) or Nikon-NSIM (100X objective, 1.4NA) with an Andor EMCCD camera controlled by NIS-Elements software. Three-dimensional invasion through collagen was visualized with an Olympus Spinning Disk microscope (20X air, 0.4NA).

Spheroid cortex fluorescence quantification

Quantifications of 2D spheroids plated on a thin layer of collagen was performed using a custom-designed Matlab script (Mathworks, Natick, MA). A maximum intensity projection of 20 z-slices was extracted from each of the images and converted to 16-bit grayscale before enhancing the pixel intensity (Matlab command: `histeq`). The enhanced image was then segmented into foreground and background using the Chan-Vese method (`activecontour`), followed by filtering of small regions (`bwareaopen`), and morphological erosion (`imerode`). The boundary from this object was then obtained (`bwboundary`) and average background intensity was subtracted. This method was used for more than 80% of the images. If this boundary did not accurately reflect the shape of the spheroid, a manual tracing option was used. This option allowed the user to select a region of interest surrounding the outer edge of the spheroid (`roipoly`). Anything outside of this boundary was masked and subsequently not considered (`regionfill`). Following this, a similar binarization/background subtraction regime was implemented on the unmasked region and the boundary was traced.

For each point along the boundary, a line perpendicular to the edge was computed and the intensity along this line was used to linearize the cortex. The resultant matrix was converted into a grayscale image. The Hough Transform was used to determine the continuity of the actin belt along the edge of the cortex. Linearized cortex images were binarized using a threshold chosen to best differentiate belt from non-belt for each set of images (`imbinarize`), followed by filtering of small regions (`bwareaopen`), and morphological dilation (`imdilate`). The Hough Transform was performed on this image (`hough`), and Hough peaks and lines identified (`houghpeaks`, `houghlines`). These were used to create a continuity score defined by $(\sum \text{Hough line lengths}) / (\text{number of lines} + \text{length of image})$. In this metric, higher scores indicate a more continuous actin belt at the cortex. Additionally, we computed a coarseness index of the cortex (`std2`) to describe actin distribution, the percentage of white pixels of the binarized image to characterize actin belt thickness, and the ratio of white pixels to gray pixels (greater than 0.15) to describe the distribution of fluorescence.

Mouse studies

Hemi-splenectomies

Hemi-splenectomies were performed on athymic *NCr-nu/nu* mice (Charles River Laboratories) with low passage AsPC-1 cells as previously described (6). In short, laparotomies were performed on anesthetized mice in which the upper pole of a divided spleen was reinserted into the peritoneum while 1×10^7 AsPC-1 cells prepared in phosphate buffered saline were injected into the lower splenic pole, chased by an equal volume of phosphate buffered saline. The pancreas and splenic vessels were ligated and the peritoneum was closed.

AsPC-1 cells were pretreated with 50 μ M 4-HAP or PBS 24 hr prior to injection during hemisplenectomies. Mice were also weighed and treated intraperitoneally with 200 μ l of 5 mg/ml of 4-HAP or 200 μ l PBS two days prior to surgery, and then treatment was continued every other day, starting on day 1 post-surgery. Mice were sacrificed upon spontaneous death of the first mouse. Samples from the mice of both this study and the survivability study were harvested as described below.

Livers were washed, weighed, photographed, and fixed in 10% formalin in PBS for 48 hrs, embedded in paraffin blocks, and sectioned as 4- μ m thick slides. Mice were housed and handled according to approved Institutional Animal Care and Use Committee protocol #M014M94.

Mouse liver tumor quantification

Quantifications of mouse livers were performed using a custom-designed Matlab script. RGB images were first separated into their three component channels. The imageSegmenter tool on Matlab was used to segment the individual channels identifying the area of the whole liver, the area of the tumor, and the area/location of the glare on the images, which was removed from the tumor area. The percent coverage of tumor was calculated.

References

1. Jhaveri DT, Kim MS, Thompson ED, Huang L, Sharma R, Klein AP, *et al.* Using Quantitative Seroproteomics to Identify Antibody Biomarkers in Pancreatic Cancer. *Cancer Immunol Res* **2016**;4:225-33
2. Jana SS, Kim KY, Mao J, Kawamoto S, Sellers JR, Adelstein RS. An alternatively spliced isoform of non-muscle myosin II-C is not regulated by myosin light chain phosphorylation. *J Biol Chem* **2009**;284:11563-71
3. Otto O, Rosendahl P, Mietke A, Golfier S, Herold C, Klaue D, *et al.* Real-time deformability cytometry: on-the-fly cell mechanical phenotyping. *Nat Methods* **2015**;12:199-202
4. Kee Y-S, Robinson DN. Micropipette Aspiration for Studying Cellular Mechanosensory Responses and Mechanics. *Dictyostelium Protocols II: Methods Mol Biol* **2013**;983:367-82
5. Mokbel M, Mokbel D, Mietke A, Träber N, Girardo S, Otto O, *et al.* Numerical Simulation of Real-Time Deformability Cytometry To Extract Cell Mechanical Properties. *ACS Biomater Sci Eng* **2017**
6. Soares KC, Foley K, Olino K, Leubner A, Mayo SC, Jain A, *et al.* A preclinical murine model of hepatic metastases. *J Vis Exp* **2014**:51677

Table S1. NMII Concentration (n), nM

Cell Line	NMIIA	NMIIB	NMIIC
HPDE	543 ± 73.8 (9)	46.2 ± 10.7 (8)	13.7 ± 1.55 (5)
Panc 4.03	774 ± 107 (10)*	7.10 ± 4.26 (10)**	19.9 ± 1.98 (5)*
Panc 10.05	563 ± 140 (8)	undetected (n/a)	18.0 ± 0.278 (5)*
AsPC-1	565 ± 141 (7)	undetected (n/a)	18.0 ± 1.05 (5)*
HeLa	550 ± 53.1 (10)	118 ± 4.72 (9)	undetected (n/a)

*p<0.05, **p<0.005, compared to HPDE

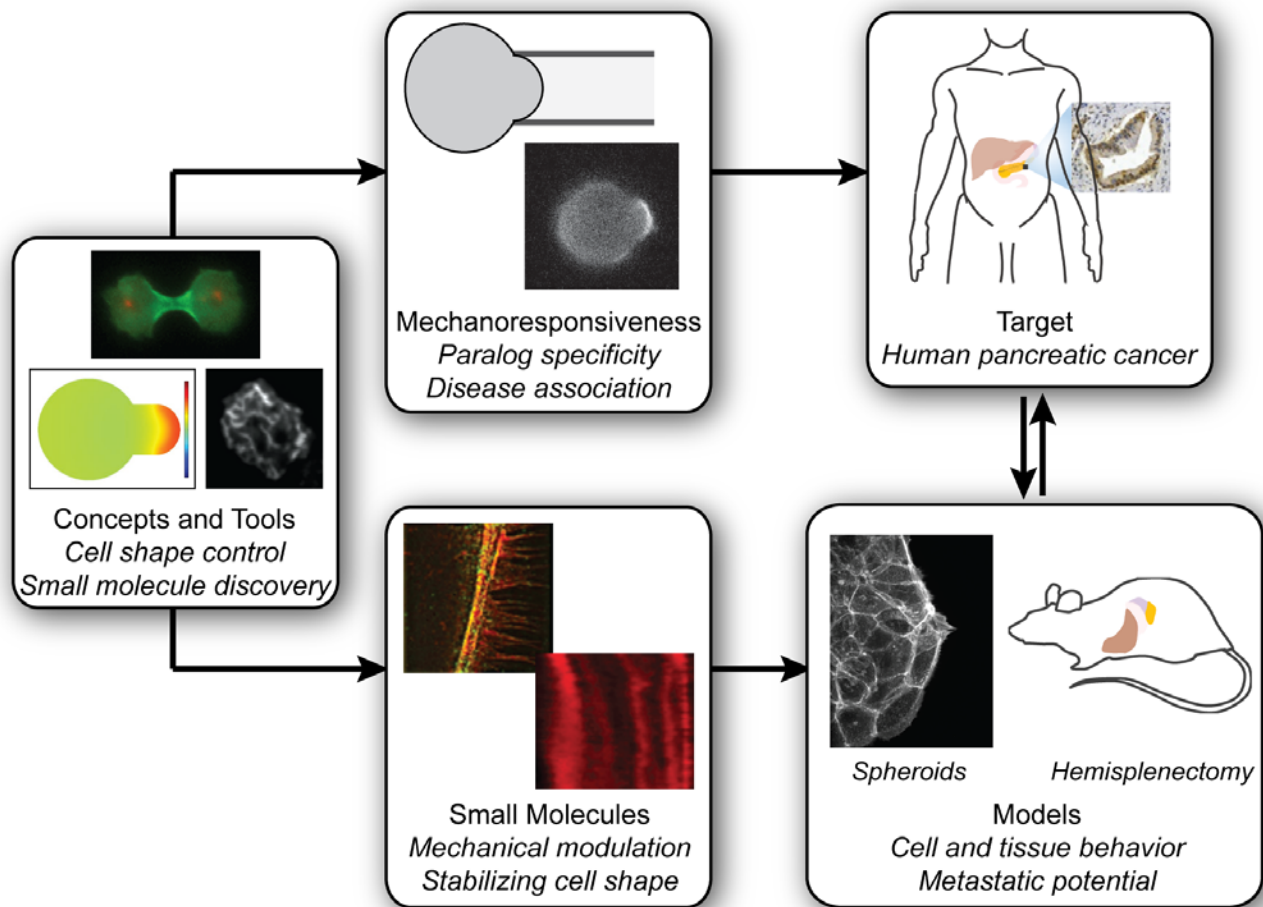


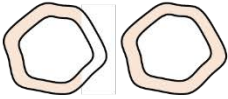

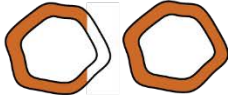
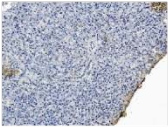
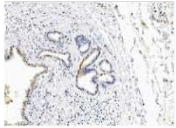
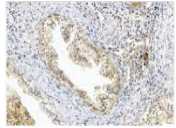
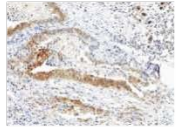
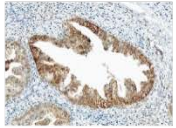


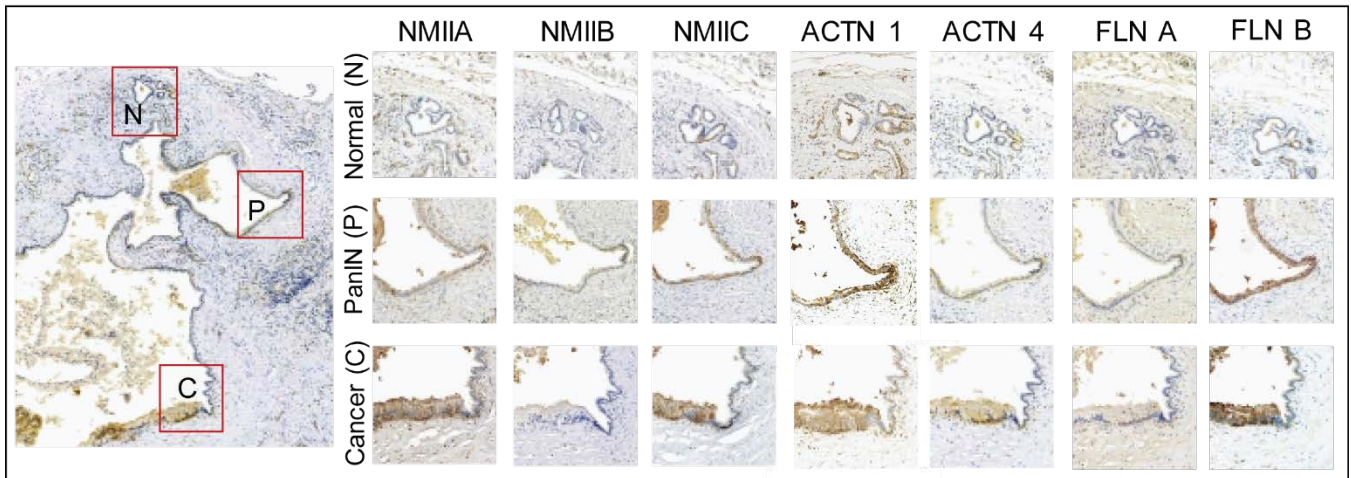
Fig. S1. Model systems to human pancreatic cancer. We have integrated our findings across models to access a targetable drug space for pancreatic ductal adenocarcinoma. We draw upon the molecular mechanisms of mechanoresponsiveness to design strategies for stabilizing the cellular dynamics that underlie metastatic potential. **Concepts and Tools:** We developed the underlying fundamental concepts for cell shape control, coupled with the identification of proteins involved in mechanical feedback regulation (mechanoresponsiveness), by studying cell division in *Dictyostelium*. This system also provided the framework for small molecule discovery used to modulate cell and tissue mechanics. **Mechanoresponsiveness:** Based on the molecular mechanisms of mechanoresponsiveness, we could predict paralog specificity of the human counterparts; those which are highly mechanoresponsive are also highly upregulated in pancreatic ductal adenocarcinoma. **Small Molecules:** A myosin II modulator 4-HAP, which we first identified in our screen using *Dictyostelium*, promotes myosin IIB and IIC assembly and

drives myosin IIC-actin transverse arcs with inhibited retrograde flow. **Models:** In human pancreatic cancer cell spheroids, 4-HAP promotes the formation of transverse actin belts, which are associated with reduced dissemination. Myosin IIA knockdown promotes increased dissemination capability, which 4-HAP can overcome. In mouse hemisplenectomy assays, 4-HAP can reduce the metastatic burden of human pancreatic cancer cells. **Target:** The goal is to decrease mortality among human pancreatic cancer patients. By combining concepts revealed in our models, which cover the dynamics, cell shape control, mechanoresponsiveness, and motility conserved in human cancer cells, we have uncovered a targetable drug space. PDAC's mechanobiome here, is targetable through the upregulation of myosin IIC and the discovery of 4-HAP, a myosin IIC modulator. Similar strategies can be employed with other elements of the mechanobiome.

A

Schematic of Ductal Intensity and Area					
Intensity/Area	0/0	1/1	1/2	2/1	2/2
Assigned Value	1	2	3	4	5
Sample Image					

B



C

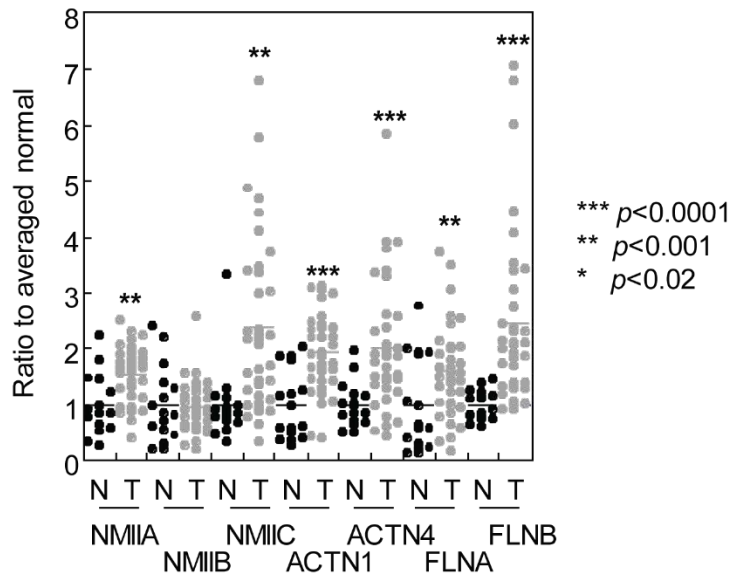


Fig. S2: Scoring analysis and differential expression patterns of mechanoresponsive and non-mechanoresponsive paralogs in patient-derived IHC data. (A) Schematic of scoring analysis of ducts from IHC data. Each analyzed duct is assigned an intensity/area value. Ducts with no staining are assigned 0/0, ducts with low intensity in less than 50% of the surface area of the duct are assigned a 1/1, ducts with low intensity staining in over 50% of the duct are given 1/2, ducts with high intensity staining in less than 50% of their surface area are assigned a 2/1, and those with high intensity in more than 50% of the duct are given a 2/2. These numbers are converted to an assigned value of 1, 2, 3, 4, and 5 respectively to be quantitatively assessed (**Fig. 2**). The sample images shown below for each assigned value are from a single patient and stained with myosin IIC antibody. (B) Sample from a duct with PanIN progression shows similar pattern of expression across all stained proteins where highly mechanoresponsive proteins (NMIIA, NMIIC, ACTN4, FLNB) increase, while non-mechanoresponsive proteins (NMIIB, FLNA) are poorly expressed or start high and remain high (ACTN1). Insets of normal (N), panIN (P), and cancerous (C) sections of the duct are presented. (C) Gene Expression Omnibus (GEO) data roughly correlates with the IHC data showing the upregulation of mechanoresponsive proteins of the PDAC mechanobiome. Normal (N) samples are compared to tumor samples (T) as normalized values to the average of the normal set within each gene. Means are provided; * $p < 0.02$, ** $p < 0.001$, *** $p < 0.0001$.

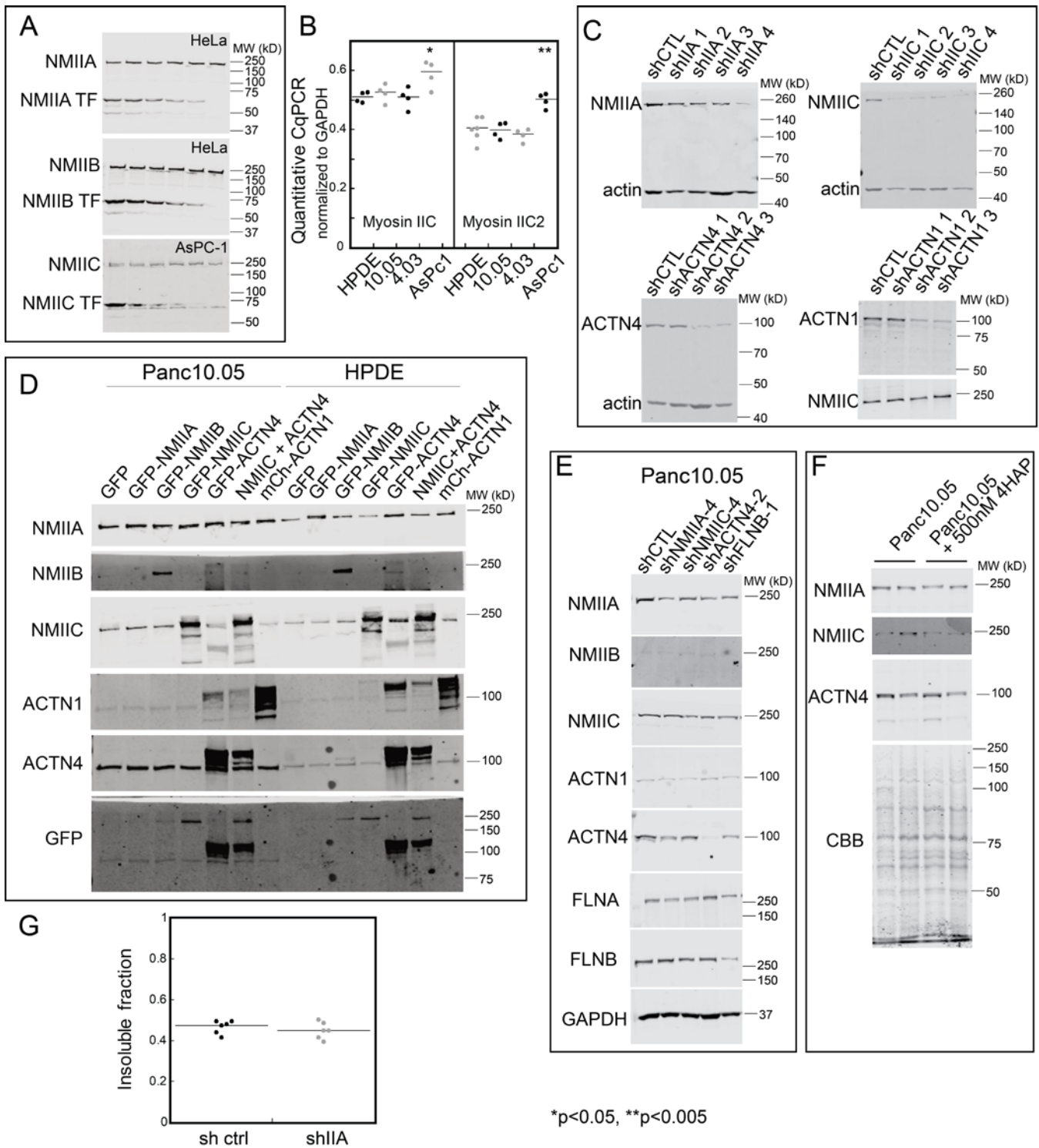


Fig. S3: Measurement of endogenous expression of nonmuscle myosin II paralogs and the effect of knockdown, overexpression, and 4-HAP treatment on the expression of mechanobiome proteins. (A) Expression of myosin IIA (NMIIA), myosin IIB (NMIIB), and myosin IIC (NMIIC) was measured by comparing endogenous expression (upper band) to a

standard curve of purified antibody epitope (lower band) added to HeLa or AsPC-1 cell extracts. **(B)** By quantitative PCR, both myosin IIC splice variants (myosin IIC and myosin IIC2) increase in expression in AsPC-1 cells. Medians are provided. **(C)** Knockdown of NMIIA, NMIIC, ACTN4, and ACTN1 using multiple shRNA constructs was confirmed by western analysis compared to a loading control (actin or NMIIC). **(D)** Overexpression of GFP-NMIIA, GFP-NMIIB, GFP-NMIIC, GFP-ACTN4, or mCherry-ACTN1 was verified by western analysis in HPDE and Panc10.05 cell lines. **(E)** Knockdown of NMIIA, NMIIC, ACTN4, and ACTN1 does not alter the expression of the other NMII and ACTN paralogs. **(F)** Overnight 4HAP treatment does not affect the expression of NMIIA, NMIIC, or ACTN4 in Panc10.05 cells (even loading verified by Coomassie Brilliant Blue staining). **(G)** Knockdown of myosin IIA (shIIA) in Panc10.05 cells did not alter the insoluble fraction (reflecting the assembled fraction) of myosin IIC. Medians are provided.

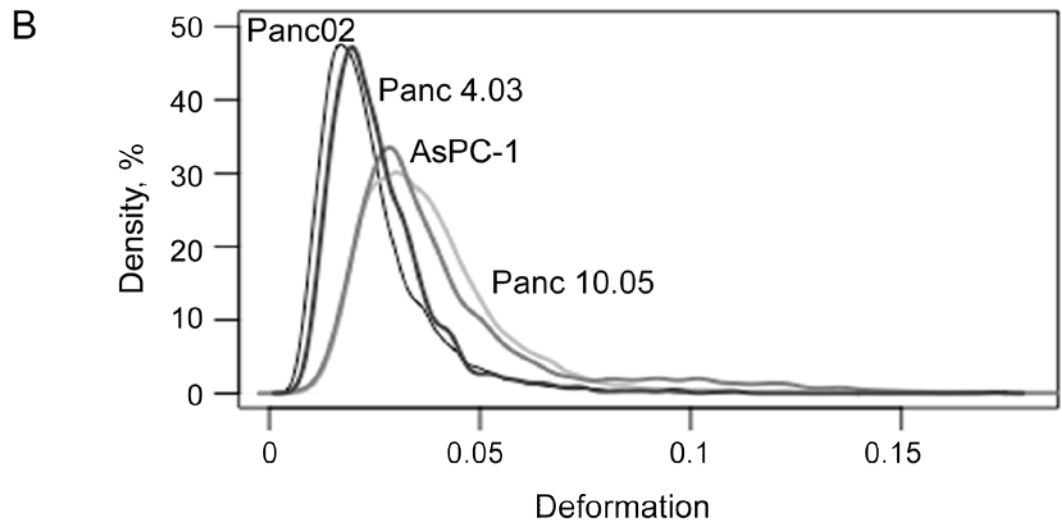
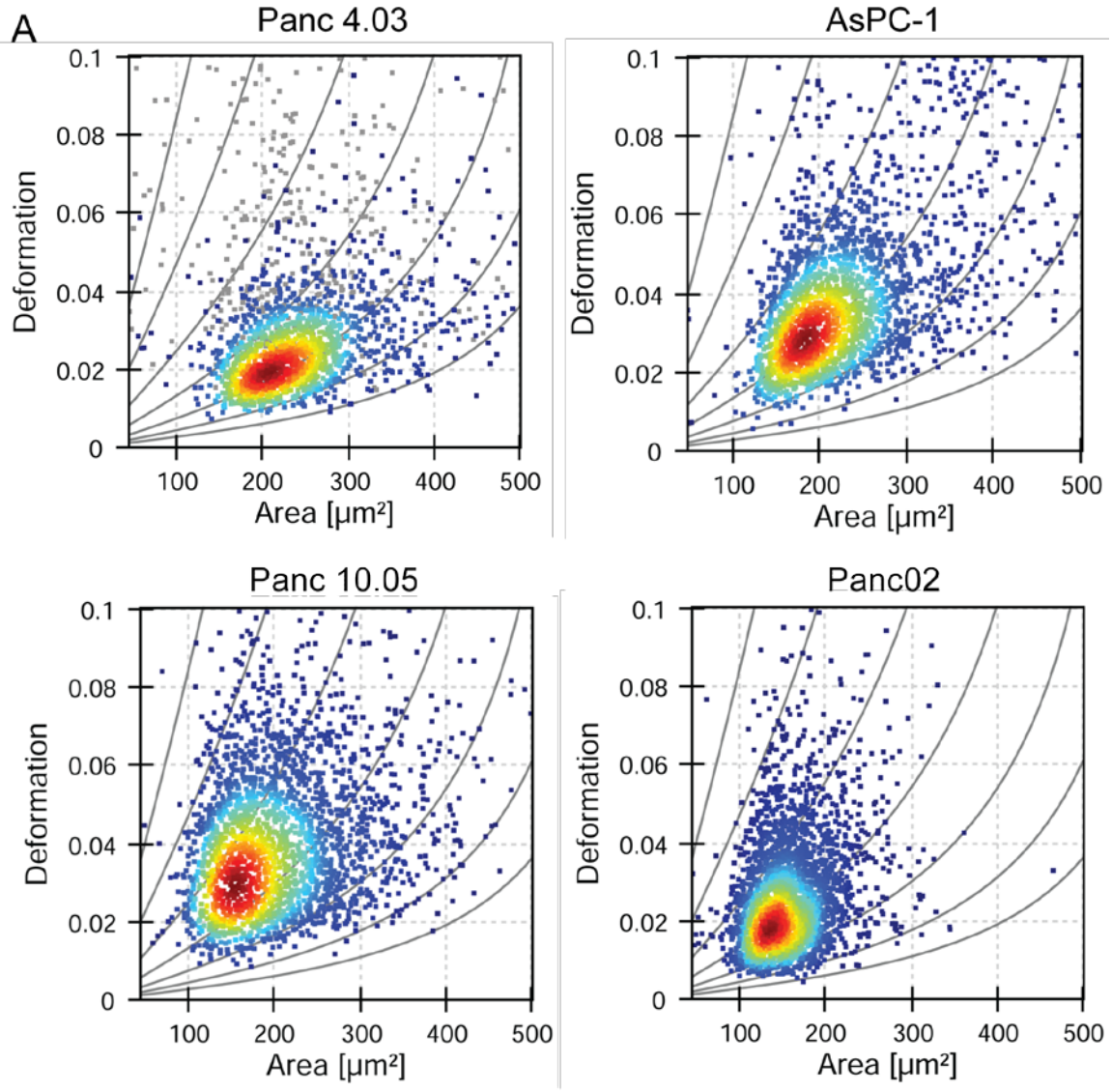


Fig. S4: Pancreatic cancer cell lines are mechanically distinct from each other. (A) RT-DC allows short-timescale cell deformation (4-ms timeframe) and cell area of thousands of cells to be rapidly measured. AsPC-1, Panc02, Panc4.03, and Panc10.05 have different degrees of deformation, likely reflecting the accumulating genetic lesions associated with the different stages of PDAC progression from which each cell-line was derived. (B) Density plots of deformation for each cell type demonstrate distinct mechanical signatures.

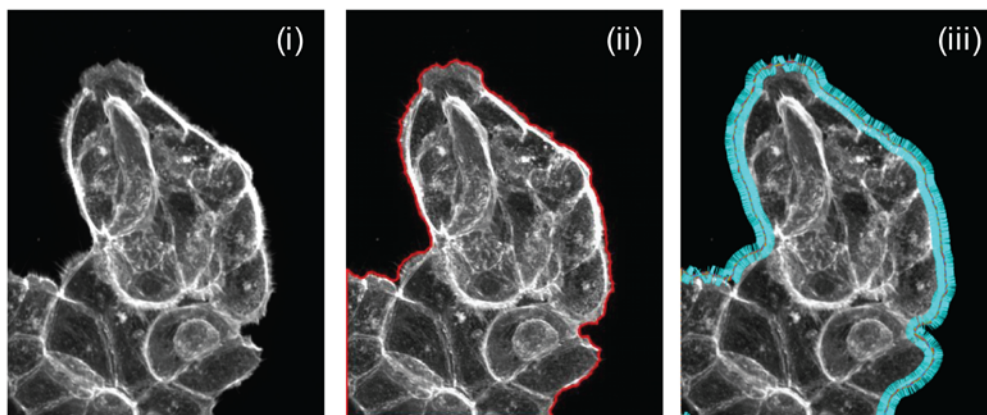
A

Steps:

Remove background (i)

Trace boundary (ii)

Draw normal lines (iii)



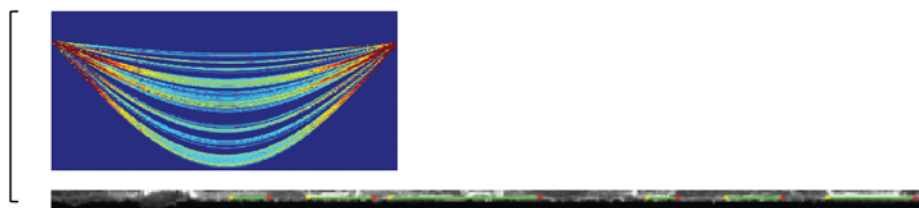
Crop the linearized boundary



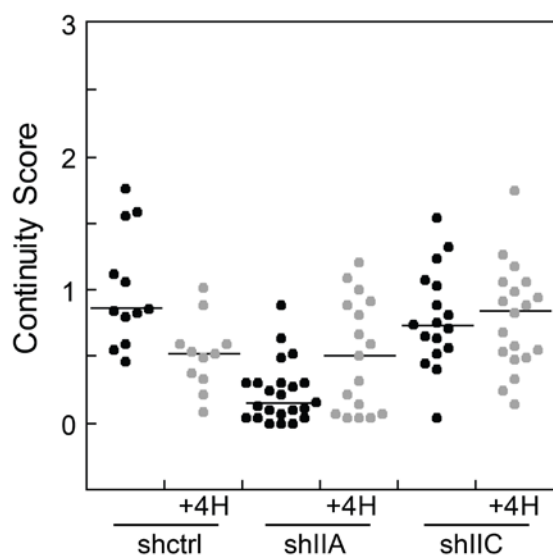
Binarize the cropped image



Hough transform to find lines



B



C

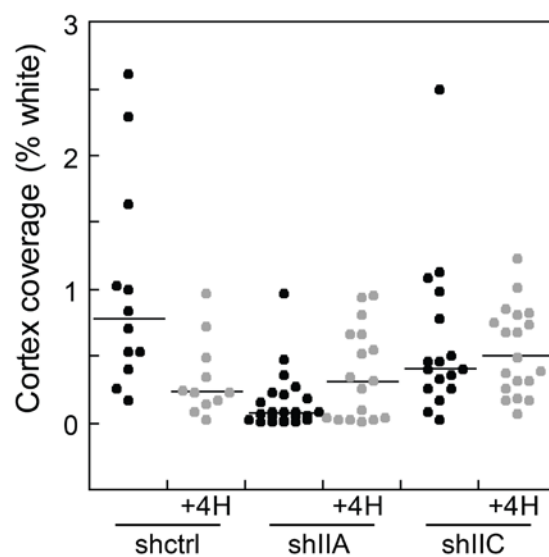


Fig. S5: Method for quantifying actin structures at the cellular cortex. (A) Sample spheroid illustrating the workflow to achieve the final linearized cortex used for quantifications. After

background subtraction (i), the edge of the spheroid was traced (ii). Normal lines were drawn from each pixel on the border (iii) to generate a linearized version of the cortex. This image was then cropped and binarized. A Hough Transform was performed on the binarized image to detect lines representing the fluorescently labeled actin bands. **(B)** From the Hough Transform we calculated a continuity score. The score is calculated by summing the lengths of the Hough lines and dividing by the number of individual Hough bands added to the length of the image. A high score indicates a more continuous actin band. The score for the control spheroids decreased upon treatment with 4-HAP, indicating an altered actin distribution upon 4-HAP treatment. The myo IIA knockdowns (shIIA) had the lowest score signifying the least continuous actin bands. Upon 4-HAP treatment, the continuity score for the shIIA cells increased significantly ($p=0.01$), indicating an increase in band continuity. The myo IIC (shIIC) knockdowns had a high score indicating a high degree of continuity, but were not affected by 4-HAP treatment indicating that 4-HAP requires myosin IIC for its action. **(C)** From the binarized cortex, additional metrics can be used to describe the cytoskeletal structure including cortex coverage defined by (number of white pixels/total number of pixels). Higher cortex coverage is roughly proportional to how much of the cortex is covered by actin bands and how thick these bands are. Control spheroids treated with 4-HAP had decreased cortex coverage, indicating an altered actin distribution. The myo IIA knockdowns had the lowest actin band coverage, but when treated with 4-HAP, the coverage increased. The myo IIC knockdowns were unaffected by the treatment of 4-HAP, but had significantly higher actin band coverage compared to the myo IIA untreated knockdowns. For B and C, medians are provided.

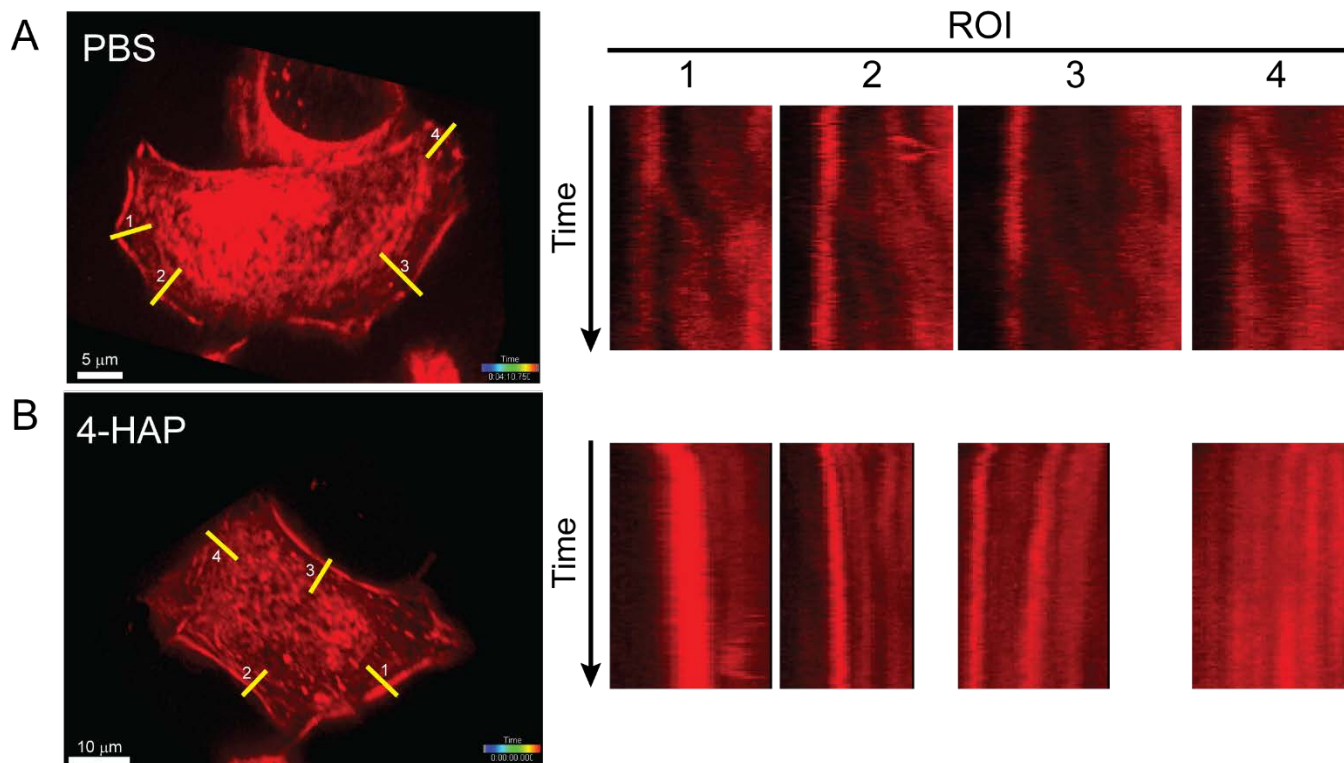


Fig. S6: 4-HAP decreases actin retrograde flow. (A) Untreated AsPC-1 cell labeled with SirAct, corresponding to **Sup. Movie 1**. (B) AsPC-1 cell treated with 4-HAP and labeled with SirAct, corresponding to **Sup. Movie 2**. Kymographs from four regions of interest (ROI) displayed on the right correspond to the four line scans (yellow) in the images on the left. Kymographs are length adjusted so that time-scale matched across the cells. Scale bars are shown on the images on the left.

A

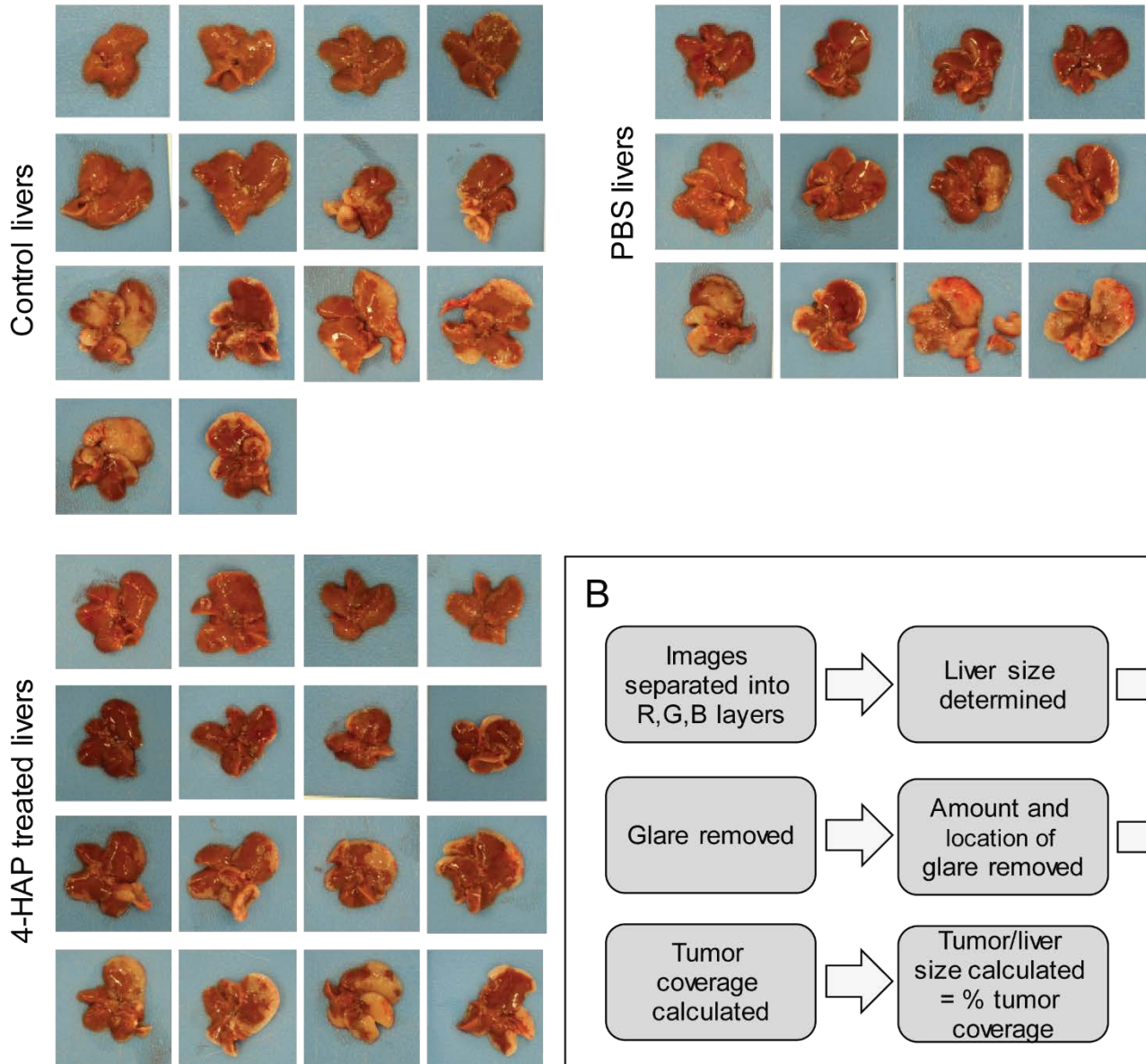


Fig. S7: 4-HAP treated livers show reduced surface tumor coverage. (A) All livers harvested from mice that underwent hemi-splenectomies are shown. **(B)** Work-flow diagram of quantification of tumor burden shown in main text **Fig. 6**.

Supplemental Movie Legends

Movie S1. Retrograde flow of an untreated AsPC-1 Sir-Act-stained cell. Data collected at 2.125 sec/frame; playback at 51 frames/sec.

Movie S2. Retrograde flow of a 4-HAP-treated AsPC-1 Sir-Act-stained cell. Data collected at 2.5 sec/frame; playback at 60 frames/sec.